

## Inhibition of the Sodium-Potassium-Chloride Cotransporter Isoform-1 Reduces Glioma Invasion

Brian R. Haas and Harald Sontheimer

### Abstract

Malignant gliomas metastasize throughout the brain by infiltrative cell migration into peritumoral areas. Invading cells undergo profound changes in cell shape and volume as they navigate extracellular spaces along blood vessels and white matter tracts. Volume changes are aided by the concerted release of osmotically active ions, most notably  $K^+$  and  $Cl^-$ . Their efflux through ion channels along with obligated water causes rapid cell shrinkage. Suitable ionic gradients must be established and maintained through the activity of ion transport systems. Here, we show that the Sodium-Potassium-Chloride Cotransporter Isoform-1 (NKCC1) provides the major pathway for  $Cl^-$  accumulation in glioma cells. NKCC1 localizes to the leading edge of invading processes, and pharmacologic inhibition using the loop diuretic bumetanide inhibits *in vitro* Transwell migration by 25% to 50%. Short hairpin RNA knockdowns of NKCC1 yielded a similar inhibition and a loss of bumetanide-sensitive cell volume regulation. A loss of NKCC1 function did not affect cell motility in two-dimensional assays lacking spatial constraints but manifested only when cells had to undergo volume changes during migration. Intracranial implantation of human gliomas into severe combined immunodeficient mice showed a marked reduction in cell invasion when NKCC1 function was disrupted genetically or by twice daily injection of the Food and Drug Administration–approved NKCC1 inhibitor Bumex. These data support the consideration of Bumex as adjuvant therapy for patients with high-grade gliomas. *Cancer Res*; 70(13); 5597–606. ©2010 AACR.

### Introduction

Among the most difficult cancers to treat, gliomas are primary brain tumors derived from glial cells. Their unusual propensity to diffusely invade surrounding brain makes complete surgical resection impossible (1). Unlike other cancers, which spread hematogenously, gliomas actively migrate along blood vessels or white matter tracts (2). The narrow extracellular spaces require invading glioma cells to undergo dynamic changes in cell shape and volume, which has been suggested to be accomplished partially by ion channel activity (3, 4). It has been postulated that invading tumor cells may shrink their leading processes while moving into narrow spaces by coordinating the release of  $K^+$  and  $Cl^-$  along with osmotically obligated water. These ions may be released through ion channels or transporters; research on glioma cells suggests that invading glioma cells primarily use ion channels for this process (5–8). Therefore, cells must establish and maintain suitable ionic gradients for  $K^+$  and  $Cl^-$ . Due

to  $Na^+/K^+$ -ATPase activity, cytoplasmic  $[K^+]$  is high, creating an outward gradient for  $K^+$  in most living cells. However, this is not true for  $Cl^-$  ions. Indeed, most neurons do not maintain a significant gradient for  $Cl^-$  ions, which instead are thought to be distributed at equilibrium. Recent studies evaluating immature neurons, astrocytes, and gliomas concluded that  $Cl^-$  ions accumulate intracellularly, establishing an outwardly directed gradient for  $Cl^-$ . Direct measurements using  $Cl^-$ -specific indicators suggest that  $Cl^-$  concentrations may be as high as 100 mmol/L in immature neurons (9), 40 mmol/L in astrocytes (10), but only around 6 to 10 mmol/L in mature neurons (11). In immature neurons, this explains why the activation of  $\gamma$ -aminobutyric acid-gated  $Cl^-$  channels causes depolarization of the cell membrane. We recently showed that  $Cl^-$  is maintained  $\sim 100$  mmol/L in glioma cells (12) and that the electrochemical gradient for  $Cl^-$  provides the energetic driving force for cell shrinkage as cells invade (12). The high intracellular  $[Cl^-]$  in gliomas is probably achieved through the action of the Sodium-Potassium-Chloride Cotransporter Isoform 1 (NKCC1; ref. 13). NKCC1 is ubiquitously expressed in most tissue types, aiding in cell volume regulation (14). It couples the influx of  $Na^+$ ,  $K^+$ , and  $2Cl^-$ , using the inward gradient for  $Na^+$  for the uphill transport of two  $Cl^-$ . NKCC1 is sensitive to bumetanide, a loop diuretic, used under the trade name Bumex, for the treatment of patients with severe renal failure (15–17).

In this study, we investigate the contribution of NKCC1 to glioma cell migration and invasion hypothesizing that NKCC1 activity establishes a gradient for  $Cl^-$  necessary to support cell volume changes required of invading glioma

**Authors' Affiliation:** Department of Neurobiology, Center for Glial Biology in Medicine, University of Alabama at Birmingham, Birmingham, Alabama

**Note:** Supplementary data for this article are available at Cancer Research Online (<http://cancerres.aacrjournals.org/>).

**Corresponding Author:** Harald Sontheimer, 1719 6th Avenue South, CIRC 425, Birmingham, AL 35294. Phone: 205-975-5805; Fax: 205-975-6320; E-mail: sontheimer@uab.edu.

doi: 10.1158/0008-5472.CAN-09-4666

©2010 American Association for Cancer Research.

cells. Under conditions mimicking the spatial constraints encountered *in vivo*, we show that NKCC1 localizes to the leading edges of migrating cells and pharmacologic inhibition of NKCC1 with the loop diuretic, bumetanide, reduces glioma cell migration. Furthermore, we show that the genetic knockdown of NKCC1, using short hairpin RNA (shRNA) constructs, inhibits cellular volume regulation and eliminates bumetanide-sensitive migration. Implantation of human glioma cells into immunocompromised severe combined immunodeficient (SCID) mice shows significantly reduced cellular invasion in animals chronically treated with bumetanide or implanted with NKCC1 knockdown cells. These data suggest the Food and Drug Administration (FDA)-approved loop diuretic bumetanide or related compounds could be considered for clinical use in patients with invasive malignant gliomas.

## Materials and Methods

### Cell culture

Experiments were performed using glioma cell lines D54-MG (glioblastoma multiforme, WHO grade IV; Dr. D. Bigner, Duke University, Durham, NC) and U87-MG [glioblastoma multiforme, WHO grade IV, American Type Culture Collection (ATCC), passaged < 4 mo]. The D54 line has not recently been authenticated. Cell cultures were maintained in DMEM/F12 (Invitrogen), supplemented with 2 mmol/L L-glutamine (CellGro) and 7% fetal bovine serum (FBS; Aleken Biologicals). Glioma cells were kept at 37°C in a 90% O<sub>2</sub>/10% CO<sub>2</sub> humidified atmosphere. HEK293 cells (ATCC) were maintained in DMEM with 10% FBS at 37°C in a 95% O<sub>2</sub>/5% CO<sub>2</sub> humidified atmosphere.

### Solutions

NaCl bath solution (pH 7.4, osmolarity 310 ± 10 mOsm) contained the following (in mmol/L): 130 NaCl, 5.0 KCl, 10.5 glucose, 32.5 HEPES, and 1 CaCl<sub>2</sub>. Bumetanide was added to bath solutions or migration assay buffer from a 1,000 × stock solution. DMSO at its final concentration (0.1%) did not disturb cell volumes or affect volume regulation (data not shown).

### Cell volume measurements and proliferation

Cell volumes were measured as previously described (18), by electronic sizing with a Coulter counter Multisizer 3 (Beckman-Coulter). Cells were kept at 37°C in bath solution during volume regulation experiments. Relative volume measurements were calculated as a ratio to the average of five baseline measurements before hyperosmotic challenge. Proliferation assays were performed as previously described (19) in the presence or absence of varying concentrations of bumetanide (Sigma) and were measured in triplicate.

### Immunocytochemistry

D54-MG (D54) and U87-MG (U87) glioma cells were grown and fixed as previously described (19); NKCC1 antibody (Millipore) was diluted 1:100 in blocking buffer containing 0.1% Triton X-100 in PBS plus 3.3% normal goat

serum in PBS and incubated overnight at 4°C. After washing with PBS, FITC-conjugated goat anti-rabbit secondary antibodies (Molecular Probes) were diluted 1:500 in blocking buffer and incubated for 1 hour in the dark. Cells were washed twice with PBS, incubated with 4',6-diamidino-2-phenylindole (DAPI) 1:2,000 in PBS, and washed once with PBS. Coverslips were mounted on glass slides with Gel Mount aqueous mounting medium (Sigma). Fluorescent images were acquired with a Zeiss Axiovert 200 M using a ×63 oil immersion lens.

### Transwell migration assays

As prior studies (12), 8.0- or 3.0-μm pore polyethylene terephthalate track-etched membrane cell culture inserts (BD Biosciences) were prepared, and cells were allowed 5 or 12 hours (8.0- and 3.0-μm pore sizes, respectively) to migrate in the presence or absence of bumetanide. Five random fields per insert were imaged at ×20 magnification on a Zeiss Axiovert 200M. Migrated cells were counted using ImageJ (NIH Image, NIH). To visualize NKCC1 localization, migrating D54 cells were fixed, stained, and imaged as previously described (20) with a ×40 air objective. Digital zooms of a single cell were taken at 0.5-μm steps for a total of 61 images (30.5 μm) and 76 images (38 μm) for the leading and lagging edges, respectively.

### Two-dimensional scratch/migration assay

D54 or U87 glioma cells were grown to a confluent monolayer, and scratches were made using a 200-μL pipette tip. Cells recovered and migrated into the wound site for 8 hours in the presence or absence of bumetanide. Images were acquired with at ×10 magnification with a Zeiss Axiovert 200M at 0 and 8 hours. The scratch area was measured using ImageJ at both 0 and 8 hours, and quantified as a ratio of 8:0 hours.

### Western blot protocol

Cultured cells were lysed, subjected to SDS-PAGE, and transferred to polyvinylidene difluoride paper as previously described (21). Membranes were blocked in a blocking buffer (5% milk in TBS plus Tween 20) for 1 hour at room temperature. Then, the membranes were incubated in primary NKCC antibody, which recognizes both isoforms (Developmental Studies Hybridoma Bank) at 1:5,000 in blocking buffer for 30 minutes at room temperature. The membranes were washed three times for 15 minutes in 5% milk in TBS plus Tween 20 and blocked for 1 hour at room temperature. Blots were incubated with horseradish peroxidase-conjugated secondary antibodies (Santa Cruz Biotechnology) for 30 minutes at room temperature. After washing, blots were developed with Super Signal West Femto enhanced chemiluminescence (Thermo Fisher Scientific) using an Eastman Kodak Image Station 4000 MM (Kodak). NKCC immunoreactivity was normalized to actin loading control (Sigma).

### ShRNA and control stable cell lines

To knockdown NKCC1 expression, we obtained commercially available pGIPZ-lentiviral shRNAmir vectors containing

either a nonsilencing scrambled sequence that does not match any known mammalian genes (NS) or one of five hairpin sequences targeting *SLC12A2* (Open Biosystems). The hairpin sequences were as follows:

NS, 5'-TGCTGTTGACAGTGAGCGATCTCGCTTGG GCG-AGAG TAAGTA GTGAAGCCACAGATGTACTTACTCTCGCCCAAGCGAGAGTGCCCTATGCCTCGGA-3'

27, 5'-TGCTGTTGACAGTGAGCGCGGTCTATCAGTCC-TTGTAATATAGT GAAGCCACAGATGTATATTACAAG-GACTGATAGACCTTGCCCTACTGCCTCGGA-3'

141, 5'-TGCTGTTGACAGTGAGCGCGGCCCTATTGTGC-CTTTAAATTAGT GAAGCCACAGATGTAATTTAAAGG-CACAATAGGCCCTTGCCCTACTGCCTCGGA-3'

382, 5'-TGCTGTTGACAGTGAGCGCCCTACCTTCTATT-CATAAATTAGT GAAGCCACAGATGTAATTTATGAA-TAGAAGGTAAGGATGCCTACTGCCTCGGA-3'

662, 5'-TGCTGTTGACAGTGAGCGACGATGGCTTATTAAGAACAAATAG TGAAGCCACAGATGTATTTGTCT-TAATAAGCCATCGCTGCCTACTGCCTCGGA-3'

690, 5'-TGCTGTTGACAGTGAGCGCGCTTCCAGATGT-TTGCTAAATAGT GAAGCCACAGATGTATTTAGCAACATCTGAAAAGCTTGCCCTACTGCCTCGGA-3'.

D54 cells were transfected using the Amaxa Biosystems nucleofection technique, as previously detailed (22).

#### **In vivo animal studies**

All animal experiments were approved and in accordance with the Institutional Animal Care and Use Committee of the University of Alabama at Birmingham. Tumor cells ( $5 \times 10^5$ ) were stereotactically injected at a 2.5-mm depth, 2.0 to 2.5 mm left of midline, and 2.0 to 2.5 mm posterior to bregma into female C.B.-17 SCID mice, ages 6 to 8 weeks, as previously reported (23). A total of  $5 \times 10^5$  tumor cells were implanted in two 5- $\mu$ L injections. Mice were divided into two treatment groups involving twice daily injections of bumetanide (5.5mg/kg) or vehicle for 3 weeks. For knockdown cells, they were prepared as above but without randomized treatment groups. Afterwards, the brains were removed and

placed in 4% PFA overnight at 4°C. The PFA was replaced with a 10% sucrose solution in 0.1 mol/L phosphate buffer (pH 7.4; phosphate buffer contains 28.34 mmol/L  $\text{NaH}_2\text{PO}_4$  and 72.11 mmol/L  $\text{Na}_2\text{HPO}_4$ ) for 1 hour at 4°C. Brains were transferred to a 30% sucrose solution (in phosphate buffer) at 4°C until the brains sank (~30 h). Brains were embedded in O.C.T. Compound Tissue Tek (Sakura Finetek), sliced on a Leica CM 1850 UV cryostat (Leica Microsystems) into 30- $\mu$ m serial sections, and placed on Colorfrost/Plus slides (Fisher-Thermo Scientific). Slices were treated to remove O.C.T. compound and stained with H&E. Images for analysis were acquired with Olympus BX51 upright modified with a LUDL motorized stage using the  $\times 4$  objective. Every tenth section was analyzed using the Stereo Investigator software's Cavalieri estimator to calculate tumor volume (MBF Bioscience). Fluorescent images of every tenth section were acquired with the AxioVision 4.6 software (Carl Zeiss) on a Zeiss Axiovert 200M. The software is equipped with a *Length* tool function allowing the accurate measurement of distances in an image. The *Length* function was used to measure tumor invasion distance from the edge of the tumor mass.

#### **Statistical analysis**

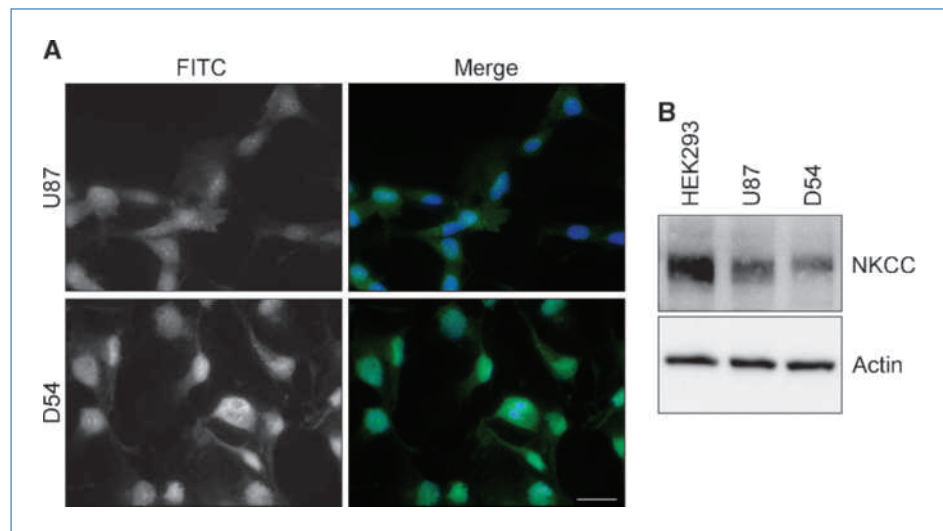
For all experiments, raw data were analyzed and graphed using the Origin 7.5 software (Microcal Software), and appropriate statistical tests were chosen according to the data analyzed using GraphPad InStat (GraphPad Software). Unless otherwise stated, all data are reported with SEM and \*, \*\*, or \*\*\* indicate  $P < 0.05$ ,  $P < 0.01$ , or  $P < 0.001$ , respectively.

## **Results**

### **Bumetanide inhibits glioma migration when space is limited**

The central hypothesis in this study posits that the NKCC1 transporter establishes ionic gradients required for rapid cell

**Figure 1.** NKCC1 is expressed in several glioma cell lines. A, immunofluorescent images of D54 and U87 glioma cells labeled with an antibody against NKCC1. The staining was repeated in triplicate three independent times. Scale bar, 20  $\mu$ m. B, example Western blot showing NKCC expression in whole-cell lysates of HEK293 (positive control), U87, and D54 cell lines with actin serving as a loading control. Full-length blots are presented in Supplementary Fig. S1.



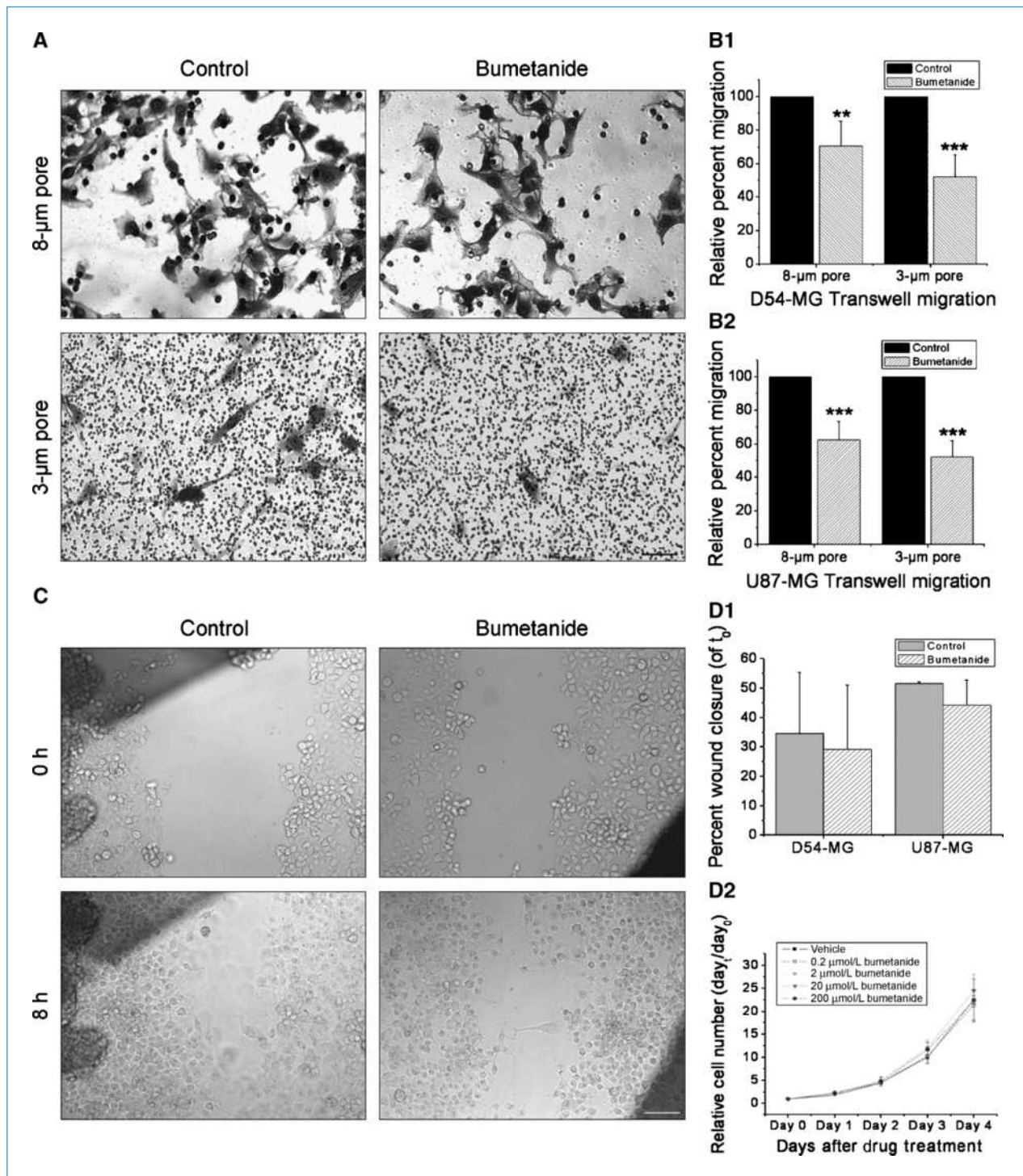


**Figure 2.** Inhibition of NKCC1 with bumetanide reduces three-dimensional migration when space is limited. **A**, representative differential interference contrast microscopy images of D54 glioma cells that have migrated through an 8- or 3- $\mu\text{m}$  Transwell barrier, for 5 or 12 h, respectively, with or without bumetanide. Scale bar, 50  $\mu\text{m}$ . **B**, **B1**, quantification of D54 glioma cell relative percent migration of on 8- and 3- $\mu\text{m}$  pore Transwell barriers. **B2**, quantification of U87 glioma cell relative percent migration on 8- and 3- $\mu\text{m}$  pore Transwell barriers. Unpaired *t* test for 8- and 3- $\mu\text{m}$  pore Transwells. Experiments were performed in triplicate and repeated five independent times. **C**, representative images of U87 glioma cells at 0 and 8 h of two-dimensional migration in the presence or absence of 200  $\mu\text{mol/L}$  bumetanide. Scale bar, 100  $\mu\text{m}$ . **D**, **D1**, quantification of percent wound closure for both D54 and U87. The experiment was performed in duplicate and repeated at least three independent times. Unpaired *t* test,  $P > 0.05$ , for D54 and U87. **D2**, D54 glioma cell proliferation in the presence or absence of the NKCC1 inhibitor, bumetanide, at four different concentrations. The experiment was completed in triplicate and repeated three independent times. One-way ANOVA,  $P > 0.05$ .

volume changes that aid the invasion of glioma cells; hence, this transporter plays an essential role in glioma invasion. To examine this question, we used several cell migration/invasion assays in which the efficacy of pharmacologic or genetic inhibitors of NKCC1 was investigated. We used two common human glioma cell lines, D54 and U87. As illustrated in Fig. 1, both cell lines showed robust NKCC1 expression as judged by immunohistochemistry (Fig. 1A) and Western blot analysis (see Supplementary Fig. S1 for full-length blots; Fig. 1B). To mimic the spatial constraints of extracellular brain space, we used 8- or 3- $\mu\text{m}$  pore Transwell migration assays. U87 and D54 glioma cells were allowed to migrate for 5 or 12 hours (8- or 3- $\mu\text{m}$  pore Transwell, respectively) in the presence or absence of bumetanide. As exhibited in Fig. 2A, bumetanide significantly inhibited D54 glioma cell migration compared with controls through 8- and 3- $\mu\text{m}$  pore Transwell barriers by approximately 25% and 50%, respectively (Fig. 2B1). A similar inhibition was found for U87 glioma cells with ~35% inhibition of migration across the 8- $\mu\text{m}$  pore Transwell barrier and 50% inhibition across the 3- $\mu\text{m}$  pore (Fig. 2B2).

Because NKCC1 is important for glioma cells' volume adjustment in constricted spaces, we would expect migration in an unrestricted environment to be less dependent on NKCC1. To test this, we assessed glioma migration in a two-dimensional wound closure assay with D54 and U87 glioma cells. Figure 2C shows example images of U87 glioma cells taken at 0 and 8 hours, in the presence or absence of bumetanide. After 8 hours, average wound closure was ~50% in U87 cells and 35% in D54, and importantly, bumetanide did not alter the wound closure significantly (Fig. 2D1), suggesting that cell motility was unaffected. To rule out any antiproliferative effects of bumetanide, D54 cells were grown for 4 days in varying concentrations of bumetanide, 0.2 to 200  $\mu\text{mol/L}$ , which did not alter population

growth throughout the experiment duration (Fig. 2D2). At day 4, there was no significant difference in the normalized cell number across all conditions. These data suggest that NKCC1 inhibition compromises cell invasion across barriers without affecting overall cell motility.

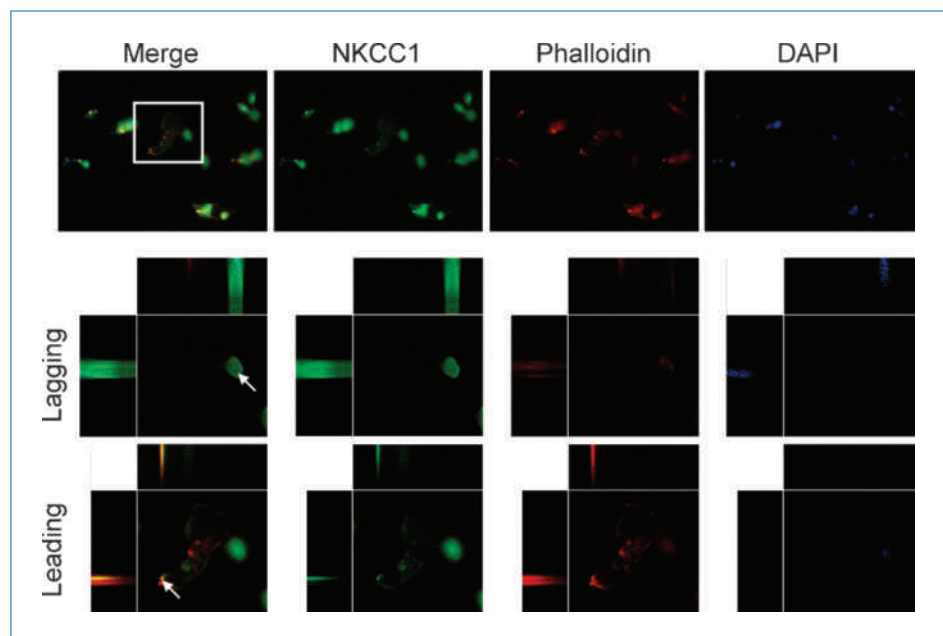
### NKCC1 localizes to the leading edge of invading glioma cells

For NKCC1 to participate in cell invasion as an influx pathway for  $\text{Cl}^-$ , it may be advantageous to localize the transporter to cell processes already past spatial constraints and in the process of enlarging their volume. We therefore examined the cellular localization of NKCC1 glioma cells fixed in the midst of traversing a Transwell barrier. As depicted in Fig. 3, the leading edges/processes of migrating D54 glioma cells showed colocalization of NKCC1 and phalloidin, whereas the lagging parts showed little to no colocalization. Separate digital magnifications of the boxed area (Fig. 3) highlight the lagging and leading edges. Arrows indicate points at which the cell is depicted in "three-view" (central panel is x,y; top panel is x,z; left panel is z,y). These data suggest that glioma cells migrating across a Transwell barrier preferentially localize NKCC1 to the membrane on leading edges of the cell.

### Genetic knockdown of NKCC1 eliminates bumetanide-sensitive migration

Although bumetanide is a fairly selective NKCC inhibitor, it has been reported to block some other transporters, most notably, the Potassium-Chloride Cotransporters (KCC; refs. 24–27). Hence, to show that the above effects were due to NKCC1 disruption and not KCC, we suppressed NKCC1 by stably transfecting D54 glioma cells with lentiviral vectors expressing five different NKCC1-knockdown shRNAs (27, 141, 382, 662, and 690), each targeting a different region

**Figure 3.** NKCC1 localizes to the membrane on the leading edge of cells migrating across Transwell barriers. First row, representative merged and individual channel images obtained at  $\times 40$ . White box, digital zoom images in the second and third rows. Second row, little to no NKCC1 (green) and phalloidin (red) colocalization on the lagging edge of a migrating glioma cell, whereas the leading edge of the same cell (third row) shows NKCC1 expression on the plasma membrane. Blue, DAPI nuclear stain. Arrows, cross-sections of cells seen in three-view through the imaging plane.



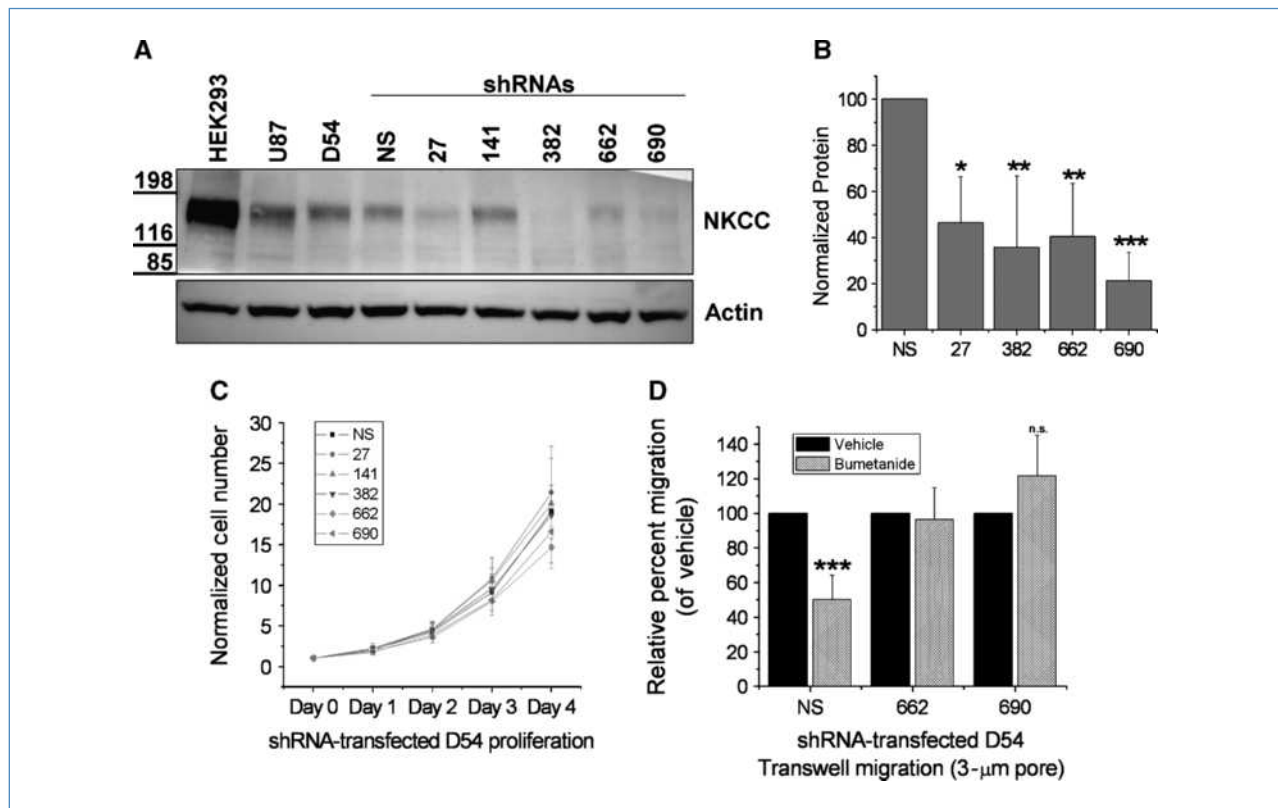


**Figure 4.** Genetic knockdown of NKCC1 has no effect on proliferation but eliminates bumetanide-sensitive migration. A, representative Western blot of whole-cell lysates of HEK293 (positive control), U87 and D54 glioma cells, and D54 glioma cells stably transfected with NKCC1 knockdowns (NS, scrambled shRNA; 27, 141, 382, 662, 690, shRNAs each targeting a different portion of the *SLC12A2* gene). Actin served as a loading control. B, quantification of NKCC1-knockdown cell line protein levels normalized to loading controls. Experiments were performed in duplicate and repeated four independent times. One-way ANOVA,  $P < 0.001$ , Tukey-Kramer *post hoc* test. C, NKCC1-knockdown cell line proliferation during 4 d. Experiments were performed in triplicate and repeated five independent times. One-way ANOVA,  $P > 0.05$ . D, quantification of NKCC1-knockdown cell line relative percent migration across a 3- $\mu$ m pore Transwell barrier. Experiments were performed in triplicate and repeated five independent times.

of the *SLC12A2* gene, or a scrambled, nonsilencing (NS) shRNA. To determine whether NKCC1 levels were effectively knocked down, protein levels from whole-cell lysates from knockdown-transfected cells were compared with NS by Western blot analysis (Fig. 4A). The NKCC antibody recognizes both isoforms, but only NKCC1 has been found in gliomas (13). HEK293 cells were used as a positive control as they express both NKCC1 and NKCC2. As shown in Fig. 4A, expression of NKCC was significantly reduced with four of the five NKCC1-knockdown shRNA constructs. After normalizing to actin, constructs 27, 382, 662, and 690 each reduced NKCC expression by at least 50% compared with NS (Fig. 4B). The shRNA construct 141, which failed to decrease NKCC expression, was not further used.

We next examined NKCC1-knockdown lines in biological assays examining growth, Transwell migration, and bumetanide sensitivity. There was no significant difference in cell proliferation between NS and all knockdowns (Fig. 4C). We then determined the ability of cells to migrate in the presence or absence of bumetanide. Employing 3- $\mu$ m pore Transwell barriers, we studied the migration of two knockdown

lines, 662 and 690, compared with NS cells. NS cell migration was inhibited by 50% in the presence of bumetanide over 12 hours (Fig. 4D), yet the two knockdown cell lines were bumetanide insensitive (unpaired *t* test,  $P > 0.05$ ). The abolishment of bumetanide-sensitive migration in knockdowns 662 and 690 along with the Western blot analysis is consistent with a loss of functional NKCC1.

#### NKCC1 blockade with bumetanide or through genetic knockdown blocks functional volume regulation

We hypothesize that during Transwell migration, cells must regulate their volume to traverse the pores involving the release of  $\text{Cl}^-$ ,  $\text{K}^+$ , and  $\text{H}_2\text{O}$ . Once successfully traversed, cells utilize NKCC1 to reestablish volume. To mimic these volume changes, we used an osmotic challenge (15 mmol/L NaCl) while monitoring cell volume changes with a Multisizer-3 Coulter Counter. The ability of glioma cells to regulate their volume back to baseline after hyperosmotic challenge is termed regulatory volume increase (RVI) and was presented in the presence or absence of 200  $\mu$ mol/L bumetanide at 37°C. Figure 5A shows that

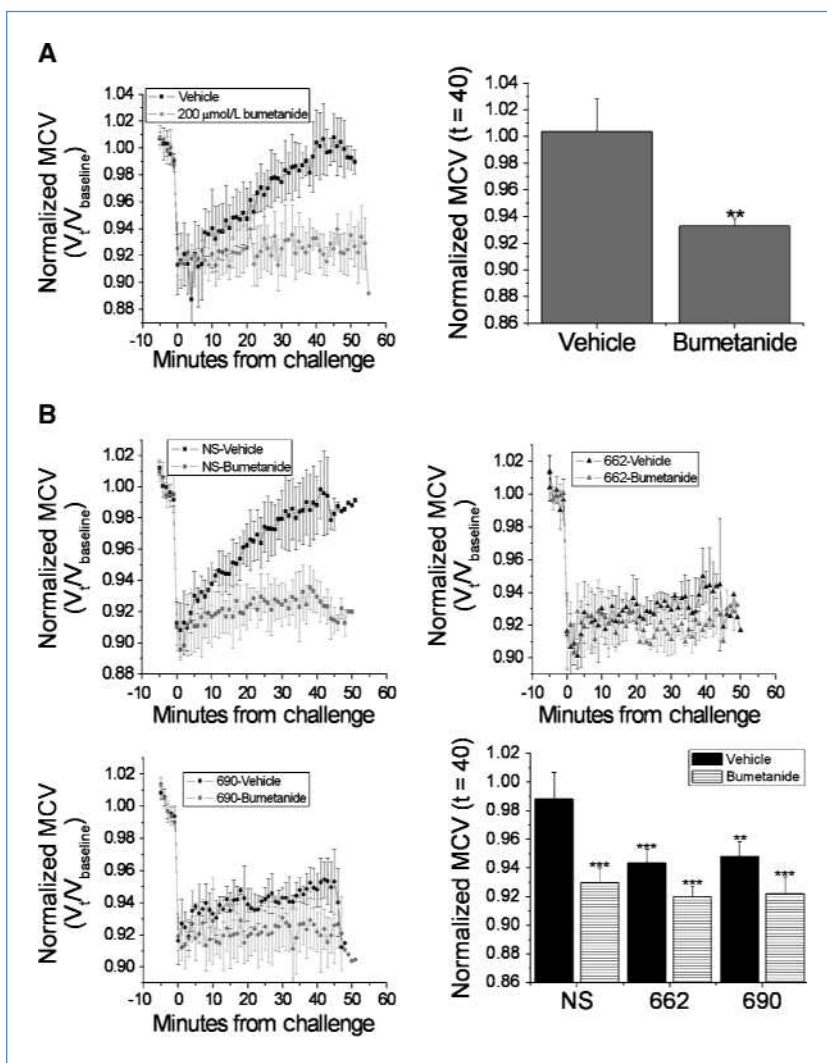
vehicle-treated D54 glioma cells undergo bumetanide-sensitive RVI, and 40 minutes postchallenge, D54 glioma cells exposed to bumetanide had failed to regulate their volume back to baseline compared with cells exposed to vehicle (Fig. 5A, right). Similarly, RVI in NS cells was completely inhibited by bumetanide, whereas both 662 and 690 knockdown cells failed to undergo RVI in the presence or absence of bumetanide (Fig. 5B). In Fig. 5B (bottom right), the normalized mean cell volumes (MCV), compared across all conditions at 40 minutes postchallenge, were significantly different from NS cells exposed to vehicle but not from each other. Together, these data confirm that genetic knockdown confers functional inhibition of NKCC1.

#### Inhibition of NKCC1 by bumetanide or stable knockdown decreases glioma cell invasion from tumors implanted into SCID mice

After assessing the effects on NKCC1 inhibition on glioma cells *in vitro*, we next investigated whether the inhibition of NKCC1 would affect glioma cell migration and invasion

*in vivo* by implanting D54 glioma cells stably transfected with eGFP (D54-eGFP), and either NS or 662, into the brains of SCID mice. Tumors were confirmed and visualized *in vivo* using an 8.5T magnetic resonance imaging (MRI) and representative images (Supplementary Fig. S2) suggest markedly reduced tumor sizes after bumetanide treatment. However, the limited spatial resolution of MRI combined with the tumor metastasis made it impossible to quantitatively assess tumor volumes by serial MRI. Therefore, we complemented these studies by assessing tumor volume with quantitative stereology. Slices were stained with H&E, and tumor volumes were determined using the Cavalieri estimator of the Stereo Investigator software (Fig. 6A). Tumor volumes were highly variable in vehicle-treated tumors, but smaller and less variable in bumetanide-treated mice. Due to the variability of the vehicle-treated group, this difference did not quite reach statistical significance ( $P = 0.06$ ; Fig. 6C1). Because our Transwell studies imply NKCC1 functions primarily to aid cell invasion, we determined the glioma cell invasiveness into peritumoral brain by measuring distances migrated from

**Figure 5.** Functional RVI is inhibited by NKCC1 blockade with bumetanide or genetic knockdown. A, left, normalized MCVs ( $n = 10,000$ – $20,000$  cells) of D54 glioma cells undergoing RVI after hyperosmotic (15 mmol/L NaCl) challenge in the presence or absence of bumetanide. Experiments were performed four independent times. Right, D54 glioma cell normalized MCVs at 40 min posthyperosmotic challenge. B, normalized MCVs for NS, 662, and 690 lines undergoing RVI after hyperosmotic challenge in the presence or absence of bumetanide. Experiments were performed four (662) or five (NS, 690) independent times. Bottom right, knockdown cell line normalized MCVs at 40 min postchallenge. One-way ANOVA,  $P < 0.05$ , Tukey-Kramer *post hoc* test.



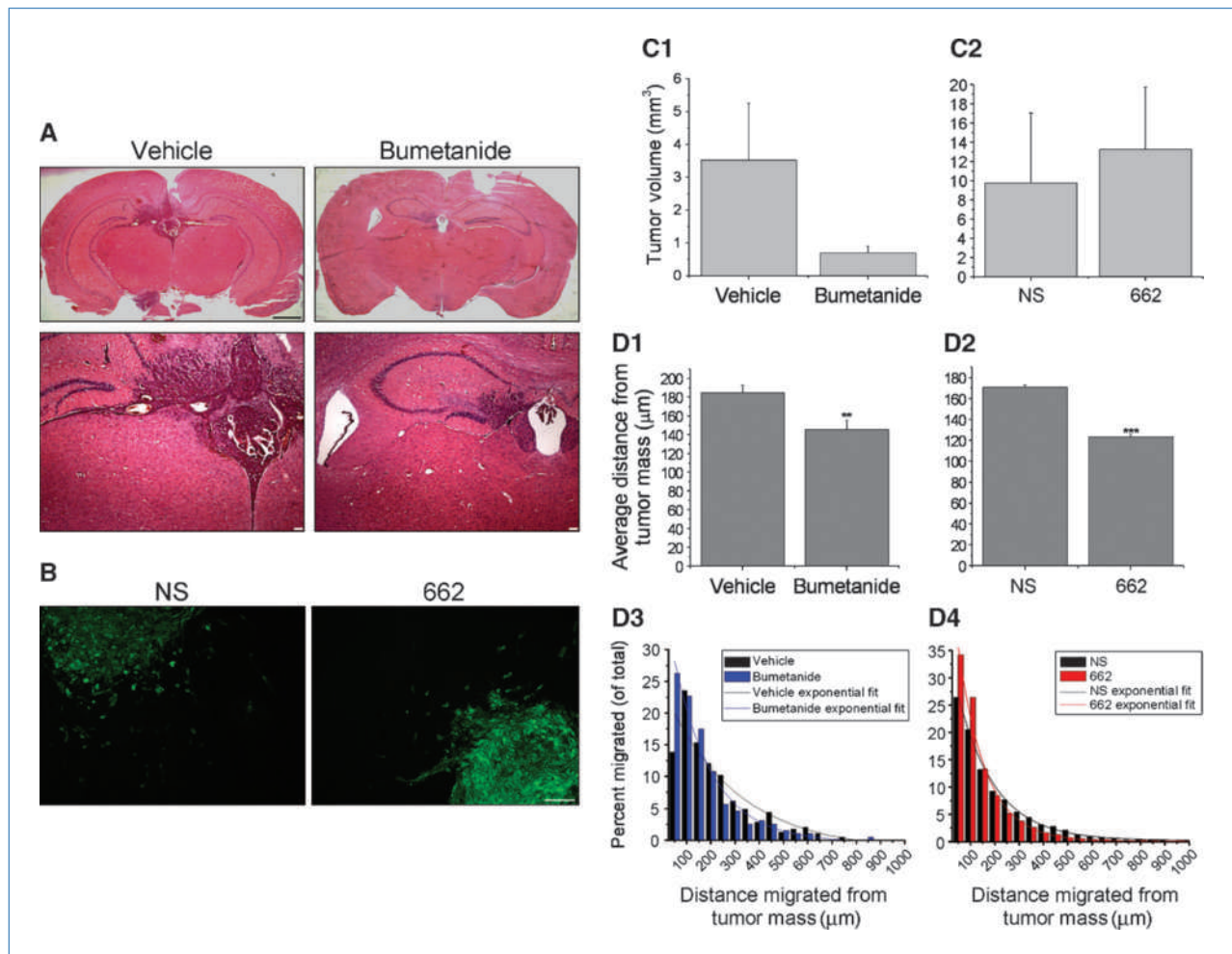


**Figure 6.** Bumetanide or NKCC1 genetic knockdown inhibits *in vivo* glioma cell invasion but not tumor size. A, examples of 30- $\mu$ m brain slices with xenografted tumor tissue stained with H&E from vehicle- or bumetanide-treated mice. Top, whole brain slice (black scale bar, 1 mm). Bottom,  $\times 4$  magnification routinely used for calculating volume (white scale bar, 100  $\mu$ m). B, immunofluorescent images of NS and 662 tumors in brain slices with cells that have migrated at various distances away from the main tumor mass. Scale bar, 100  $\mu$ m. C, quantification *in vivo* tumor volumes for D54-eGFP tumors (C1) and NKCC1-knockdowns (C2). Tumor volumes between vehicle-treated ( $n = 4$ ) and bumetanide-treated ( $n = 7$ ) tumors (C1), and between NS ( $n = 7$ ) and 662 ( $n = 8$ ) tumors (C2) were not significantly different. Unpaired  $t$  test,  $P > 0.05$ . D, tumor cell average distance migrated from primary tumor mass in vehicle-treated ( $n = 390$ ) and bumetanide-treated ( $n = 194$ ) mice (D1) and knockdowns (D2), NS ( $n = 4,591$ ) and 662 ( $n = 4,690$ ). D3, distribution of invaded D54-eGFP tumor cells from both vehicle- and bumetanide-treated tumors. The decay constants of the exponential fit curves were approximately 295 and 160 for vehicle- and bumetanide-treated groups, respectively. D4, distribution of invaded tumor cells from both NS and 662 tumors. The decay constants of the exponential fit curves were approximately 154 and 112 for NS and 662, respectively (for full equation values, see Supplementary Table S1).

the primary tumor mass. Using green fluorescent protein fluorescence, we acquired images of all visible invading cells (Fig. 6B). After measuring each invading cell(s) distance, we calculated the average distance migrated from the tumor mass (Fig. 6D1). We found a significant difference between vehicle- and bumetanide-treated tumors. We then plotted the distance of cell migration as a function of frequency of occurrence (Fig. 6D3). These data were well fit to a single exponential function. An exponential decrease in the cell number with invasion distance is predicted by Withers and Lee (28). From this function,  $y = A_1 * e^{(-x/t)} + y_0$ , one can conveniently derive the decay constants ( $t$ ) of  $295.4 \pm 78.7$  and  $160.0 \pm 12.5$  for vehicle- and bumetanide-treated tumors, re-

spectively (Supplementary Table S1 for equation values), with the Origin 7.5 software for comparison. These data suggest that roughly one third ( $1/e$ ) of the vehicle-treated tumor cells migrated at least 295  $\mu$ m from the tumor, which was almost twice that of bumetanide-treated tumors. Hence, these data indicate that bumetanide inhibits *in vivo* glioma cell invasion.

We then repeated these *in vivo* experiments using one NKCC1-knockdown cell line, 662, compared with NS cells. As before, we assessed tumor volume and found no statistical difference between NS and 662 tumor volumes (Fig. 6C2). However, when we evaluated the average distance glioma cells migrated from the tumor mass, we found a significant

decrease in invading 662 cells (Fig. 6D2). The average distance migrated from the tumor mass was significantly different at 170.74 and 123.55  $\mu\text{m}$  for NS and 662 tumors, respectively. As previously mentioned, we further examined the frequency distribution of glioma cell migration (Fig. 6D4) deriving the decay constants of  $154.0 \pm 5.3$  for NS tumors and  $111.9 \pm 6.3$  for 662 tumors. These data, from *in vivo* tumor growth, suggest NKCC1 facilitates the invasion of glioma cells.

## Discussion

In this study, we show that the disruption of  $\text{Cl}^-$  uptake through NKCC1, pharmacologically, or shRNA-knockdown inhibits glioma cell invasion. More specifically, cell migration was inhibited in three-dimensional migration assays in which cells encounter spatial constraints, yet cell motility on a two-dimensional substrate was unaffected by NKCC1 inhibition. Importantly, NKCC1 inhibition reduced cell invasion upon implantation of gliomas into SCID mice in which individual tumor cells invaded significantly less deep into the surrounding brain upon NKCC1 disruption.

These findings support the hypothesis that glioma cells undergo profound changes in cell volume as they invade brain tissue and they use  $\text{Cl}^-$  as an osmolyte to regulate cell volume while invading. Ion movement across the membrane is associated with obligatory water movement and has been shown to play a critical role in cell shape and volume changes associated with glioma cell migration (3, 12, 29, 30), and if normosmotic conditions are perturbed, glioma cell migration is significantly reduced (see Supplementary Fig. S3 and Supplementary Text). Ion movement also plays an important role in migration in other cell types. Chloride efflux through ion channels has been shown to play a major role in cell invasion. For example, in HeLa cells, pharmacological inhibition of  $\text{Cl}^-$  channels or antisense knockdown of the chloride channel  $\text{ClC-3}$  inhibits Transwell migration by 50% (31). Similar results were reported for nasopharyngeal carcinoma cells (32). Glioma cells express several members of the  $\text{ClC}$  channel family including  $\text{ClC-3}$  (33), and the  $\text{Cl}^-$  channel inhibitor 5-nitro-2-(3-phenylpropylamino)-benzoate reduces invasion (29). Consequently,  $\text{ClC-3}$  may similarly be involved in the volume changes of invading glioma cells. However, for purposes of this study, the molecular identity of the underlying  $\text{Cl}^-$  current is irrelevant. For  $\text{Cl}^-$  to act as osmolyte, it must be accumulated intracellularly and requires sustained uptake of  $\text{Cl}^-$  through NKCC1. Indeed, gliomas have been shown to accumulate  $\text{Cl}^-$  up to 100 mmol/L intracellularly (12).

Several studies (34, 35), including ones in glioma cells (22, 36), suggest that  $\text{Cl}^-$  efflux is important during defined stages of cell division, particularly preceding mitosis. We were surprised to find cell proliferation unaffected by NKCC1 disruption. It is possible that chronic NKCC1 inhibition leads to compensatory expression of alternative  $\text{Cl}^-$  transporters, for example, the  $\text{Cl}^-/\text{HCO}_3^-$  transporter AE3 (37). This may also explain why NKCC1-null mice are viable at birth (38). Despite possible compensatory mechanisms, our study shows that NKCC1 inhibition with bumetanide decreases cell migration. Although, bumetanide is a potent inhibitor of NKCC1, it could possibly affect other cation/chloride cotransporters, such as the KCCs, even with the affinity  $\text{NKCC} \gg \text{KCC}$  (27). Although the bumetanide concentration used (200  $\mu\text{mol/L}$ ) may have also inhibited KCCs, similar or even higher concentrations have previously been used by us (12, 13) and others (39–43) to selectively block NKCC1. Importantly, our data (Fig. 5) shows that NKCC1-knockdown cells are insensitive to bumetanide, suggesting that the drug targets only NKCC1 in our experiments.

We also found that invading glioma cells preferentially localize NKCC1 at the leading edge. This may suggest that  $\text{Cl}^-$  transport supports local cell volume changes, which possibly does not affect overall cell volume. An important aspect of the pharmacological effect of bumetanide on cell invasion is the fact that the drug is FDA approved (Bumex) for the treatment of kidney disease, and hence, it would have a short path to clinical use as adjuvant therapy for gliomas.

## Disclosure of Potential Conflicts of Interest

No potential conflicts of interest were disclosed.

## Acknowledgments

We thank Martin Pike for the MR imaging assistance and Susan Buckingham for animal surgical expertise. The NKCC antibody developed by Forbush and Lytle was obtained from the Developmental Studies Hybridoma Bank developed under the auspices of the National Institute of Child Health and Human Resources and maintained by The University of Iowa, Department of Biological Sciences, Iowa City, IA 52242.

## Grant Support

NIH-RO1-036692, RO1-031234, and Neuroscience Blueprint Core Grant NS57098. The costs of publication of this article were defrayed in part by the payment of page charges. This article must therefore be hereby marked *advertisement* in accordance with 18 U.S.C. Section 1734 solely to indicate this fact.

Received 12/22/2009; revised 04/12/2010; accepted 05/10/2010; published OnlineFirst 06/22/2010.

## References

- Hoelzinger DB, Demuth T, Berens ME. Autocrine factors that sustain glioma invasion and paracrine biology in the brain microenvironment. *J Natl Cancer Inst* 2007;99:1583–93.
- Giese A, Westphal M. Glioma invasion in the central nervous system. *Neurosurgery* 1996;39:235–50.
- Soroceanu L, Manning TJ, Jr., Sontheimer H. Modulation of glioma cell migration and invasion using  $\text{Cl}^-$  and  $\text{K}^+$  ion channel blockers. *J Neurosci* 1999;19:5942–54.
- Ordaz B, Vaca L, Franco R, Pasantes-Morales H. Volume changes and whole cell membrane currents activated during gradual osmolarity decrease in C6 glioma cells: contribution of two types of  $\text{K}^+$  channels. *AJP - Cell Physiol* 2004;286:C1399–1409.

5. Sontheimer HW. An unexpected role for ion channels in brain tumor metastasis. *Exp Biol Med* (Maywood) 2008;233:779–91.
6. Sontheimer H. Ion channels and amino acid transporters support the growth and invasion of primary brain tumors. *Mol Neurobiol* 2004;29:61–71.
7. Vila-Carriles WH, Kovacs GG, Jovov B, et al. Surface expression of ASIC2 inhibits the amiloride-sensitive current and migration of glioma cells. *J Biol Chem* 2006;281:19220–32.
8. Fan S, Sun Z, Jiang D, et al. BmkCT toxin inhibits glioma proliferation and tumor metastasis. *Cancer Lett* 2009;291:1158–66.
9. Kuner T, Augustine GJ. A genetically encoded ratiometric indicator for chloride: capturing chloride transients in cultured hippocampal neurons. *Neuron* 2000;27:447–59.
10. Kettenmann H, Backus KH, Schachner M.  $\gamma$ -Aminobutyric acid opens Cl<sup>-</sup> channels in cultured astrocytes. *Brain Res* 1987;404:1–9.
11. DeFazio RA, Hablitz JJ. Chloride accumulation and depletion during GABA(A) receptor activation in neocortex. *Neuroreport* 2001;12:2537–41.
12. Habela CW, Ernest NJ, Swindall AF, Sontheimer H. Chloride accumulation drives volume dynamics underlying cell proliferation and migration. *J Neurophysiol* 2009;101:750–7.
13. Ernest NJ, Sontheimer H. Extracellular glutamine is a critical modulator for regulatory volume increase in human glioma cells. *Brain Res* 2007;1144:231–8.
14. Haas M, Forbush B III. The Na-K-Cl cotransporters. *J Bioenerg Biomembr* 1998;30:161–72.
15. Asbury MJ, Gatenby PB, O'Sullivan S, Bourke E. Bumetanide: potent new "loop" diuretic. *Br Med J* 1972;1:211–3.
16. Popowicz P, Simmons NL. [<sup>3</sup>H]bumetanide binding and inhibition of Na<sup>+</sup> + K<sup>+</sup> + Cl<sup>-</sup> co-transport: demonstration of specificity by the use of MDCK cells deficient in co-transport activity. *Q J Exp Physiol* 1988;73:193–202.
17. Isenring P, Jacoby SC, Chang J, Forbush B. Mutagenic mapping of the Na-K-Cl cotransporter for domains involved in ion transport and bumetanide binding. *J Gen Physiol* 1998;112:549–58.
18. Ernest NJ, Weaver AK, Van Duyn LB, Sontheimer HW. Relative contribution of chloride channels and transporters to regulatory volume decrease in human glioma cells. *Am J Physiol Cell Physiol* 2005;288:C1451–1460.
19. Bomben VC, Sontheimer HW. Inhibition of transient receptor potential canonical channels impairs cytokinesis in human malignant gliomas. *Cell Prolif* 2008;41:98–121.
20. Cuddapah VA, Sontheimer H. Molecular interaction and functional regulation of CIC-3 by Ca<sup>2+</sup>/calmodulin-dependent protein kinase II (CaMKII) in human malignant glioma. *J Biol Chem* 2010;285:11188–96.
21. Olsen ML, Campbell SL, Sontheimer H. Differential distribution of kir4.1 in spinal cord astrocytes suggests regional differences in K<sup>+</sup> homeostasis. *J Neurophysiol* 2007;98:786–93.
22. Habela CW, Olsen ML, Sontheimer H. CIC3 is a critical regulator of the cell cycle in normal and malignant glial cells. *J Neurosci* 2008;28:9205–17.
23. Soroceanu L, Gillespie Y, Khazaeli MB, Sontheimer H. Use of chlorotoxin for targeting of primary brain tumors. *Cancer Res* 1998;58:4871–9.
24. Lauf PK, Adragna NC, Garay RP. Activation by N-ethylmaleimide of a latent K<sup>+</sup>-Cl<sup>-</sup> flux in human red blood cells. *Am J Physiol* 1984;246:C385–390.
25. Chassande O, Frelin C, Farahifar D, Jean T, Lazdunski M. The Na<sup>+</sup>/K<sup>+</sup>/Cl<sup>-</sup> cotransport in C6 glioma cells. Properties and role in volume regulation. *Eur J Biochem* 1988;171:425–33.
26. Gillen CM, Brill S, Payne JA, Forbush B III. Molecular cloning and functional expression of the K-Cl cotransporter from rabbit, rat, and human. A new member of the cation-chloride cotransporter family. *J Biol Chem* 1996;271:16237–44.
27. Gagnon KB, Adragna NC, Fyffe RE, Lauf PK. Characterization of glial cell K-Cl cotransport. *Cell Physiol Biochem* 2007;20:121–30.
28. Withers HR, Lee SP. Modeling growth kinetics and statistical distribution of oligometastases. *Semin Radiat Oncol* 2006;16:111–9.
29. Ransom CB, O'Neal JT, Sontheimer H. Volume-activated chloride currents contribute to the resting conductance and invasive migration of human glioma cells. *J Neurosci* 2001;21:7674–83.
30. Lyons SA, Chung WJ, Weaver AK, Ogunrinu T, Sontheimer H. Auto-crine glutamate signaling promotes glioma cell invasion. *Cancer Res* 2007;67:9463–71.
31. Mao J, Chen L, Xu B, et al. Volume-activated chloride channels contribute to cell-cycle-dependent regulation of HeLa cell migration. *Biochem Pharmacol* 2009;77:159–68.
32. Mao J, Chen L, Xu B, et al. Suppression of CIC-3 channel expression reduces migration of nasopharyngeal carcinoma cells. *Biochem Pharmacol* 2008;75:1706–16.
33. Olsen ML, Schade S, Lyons SA, Amarillo MD, Sontheimer H. Expression of voltage-gated chloride channels in human glioma cells. *J Neurosci* 2003;23:5572–82.
34. Tang YB, Liu YJ, Zhou JG, Wang GL, Qiu QY, Guan YY. Silence of CIC-3 chloride channel inhibits cell proliferation and the cell cycle via G/S phase arrest in rat basilar arterial smooth muscle cells. *Cell Prolif* 2008;41:775–85.
35. Yu WF, Zhao YL, Wang K, Dong MM. Inhibition of cell proliferation and arrest of cell cycle progression by blocking chloride channels in human laryngeal cancer cell line Hep-2. *Neoplasma* 2009;56:224–9.
36. Habela CW, Sontheimer H. Cytoplasmic volume condensation is an integral part of mitosis. *Cell Cycle* 2007;6.
37. Stewart AK, Yamamoto A, Nakakuki M, Kondo T, Alper SL, Ishiguro H. Functional coupling of apical Cl<sup>-</sup>/HCO<sub>3</sub><sup>-</sup> exchange with CFTR in stimulated HCO<sub>3</sub><sup>-</sup> secretion by guinea pig interlobular pancreatic duct. *Am J Physiol Gastrointest Liver Physiol* 2009;296:G1307–1317.
38. Flagella M, Clarke LL, Miller ML, et al. Mice lacking the basolateral Na-K-2Cl cotransporter have impaired epithelial chloride secretion and are profoundly deaf. *J Biol Chem* 1999;274:26946–55.
39. Kelly T, Kafitz KW, Roderigo C, Rose CR. Ammonium-evoked alterations in intracellular sodium and pH reduce glial glutamate transport activity. *Glia* 2009;57:921–34.
40. Garay RP, Nazaret C, Hannaert PA, Cragoe EJ, Jr. Demonstration of a [K<sup>+</sup>,Cl<sup>-</sup>]-cotransport system in human red cells by its sensitivity to [(dihydroindenyl)oxy]alkanoic acids: regulation of cell swelling and distinction from the bumetanide-sensitive [Na<sup>+</sup>,K<sup>+</sup>,Cl<sup>-</sup>]-cotransport system. *Mol Pharmacol* 1988;33:696–701.
41. Chen H, Sun D. The role of Na-K-Cl co-transporter in cerebral ischemia. *Neurol Res* 2005;27:280–6.
42. Tse WK, Au DW, Wong CK. Effect of osmotic shrinkage and hormones on the expression of Na<sup>+</sup>/H<sup>+</sup> exchanger-1, Na<sup>+</sup>/K<sup>+</sup>/2Cl<sup>-</sup> cotransporter and Na<sup>+</sup>/K<sup>+</sup> -ATPase in gill pavement cells of freshwater adapted Japanese eel, *Anguilla japonica*. *J Exp Biol* 2007;210:2113–20.
43. Wertheimer EV, Salicioni AM, Liu W, et al. Chloride is essential for capacitation and for the capacitation-associated increase in tyrosine phosphorylation. *J Biol Chem* 2008;283:35539–50.

# Cancer Research

The Journal of Cancer Research (1916–1930) | The American Journal of Cancer (1931–1940)

## Inhibition of the Sodium-Potassium-Chloride Cotransporter Isoform-1 Reduces Glioma Invasion

Brian R. Haas and Harald Sontheimer

*Cancer Res* 2010;70:5597-5606. Published OnlineFirst June 22, 2010.

<b>Updated version</b>	Access the most recent version of this article at: doi: <a href="https://doi.org/10.1158/0008-5472.CAN-09-4666">10.1158/0008-5472.CAN-09-4666</a>
<b>Supplementary Material</b>	Access the most recent supplemental material at: <a href="http://cancerres.aacrjournals.org/content/suppl/2010/06/22/0008-5472.CAN-09-4666.DC1">http://cancerres.aacrjournals.org/content/suppl/2010/06/22/0008-5472.CAN-09-4666.DC1</a>

<b>Cited articles</b>	This article cites 42 articles, 15 of which you can access for free at: <a href="http://cancerres.aacrjournals.org/content/70/13/5597.full#ref-list-1">http://cancerres.aacrjournals.org/content/70/13/5597.full#ref-list-1</a>
-----------------------	--

<b>Citing articles</b>	This article has been cited by 10 HighWire-hosted articles. Access the articles at: <a href="http://cancerres.aacrjournals.org/content/70/13/5597.full#related-urls">http://cancerres.aacrjournals.org/content/70/13/5597.full#related-urls</a>
------------------------	--

<b>E-mail alerts</b>	<a href="#">Sign up to receive free email-alerts</a> related to this article or journal.
----------------------	--

<b>Reprints and Subscriptions</b>	To order reprints of this article or to subscribe to the journal, contact the AACR Publications Department at <a href="mailto:pubs@aacr.org">pubs@aacr.org</a> .
-----------------------------------	--

<b>Permissions</b>	To request permission to re-use all or part of this article, use this link <a href="http://cancerres.aacrjournals.org/content/70/13/5597">http://cancerres.aacrjournals.org/content/70/13/5597</a> . Click on "Request Permissions" which will take you to the Copyright Clearance Center's (CCC) Rightslink site.
--------------------	--